drones

MDPI

Article

Comparing Filtering Techniques for Removing Vegetation from UAV-Based Photogrammetric Point Clouds

Niels Anders [1], João Valente [2,*], Rens Masselink [1] and Saskia Keesstra [3,4]

[1] Satelligence BV, Maliebaan 22, 3581 CP Utrecht, The Netherlands
[2] Information Technology Group, Wageningen University, Hollandseweg 1, 6706 KN Wageningen, The Netherlands
[3] Team Soil, Water and Land Use, Wageningen Environmental Research, PO Box 47, 6700 AA Wageningen, The Netherlands
[4] School of Engineering, Faculty of Engineering and Built Environment, The University of Newcastle, University Drive, Callaghan, NSW 2308, Australia
* Correspondence: joao.valente@wur.nl

Received: 29 June 2019; Accepted: 26 July 2019; Published: 30 July 2019

Abstract: Digital Elevation Models (DEMs) are 3D representations of the Earth's surface and have numerous applications in geomorphology, hydrology and ecology. Structure-from-Motion (SfM) photogrammetry using photographs obtained by unmanned aerial vehicles (UAVs) have been increasingly used for obtaining high resolution DEMs. These DEMs are interpolated from point clouds representing entire landscapes, including points of terrain, vegetation and infrastructure. Up to date, there has not been any study clearly comparing different algorithms for filtering of vegetation. The objective in this study was, therefore, to assess the performance of various vegetation filter algorithms for SfM-obtained point clouds. The comparison was done for a Mediterranean area in Murcia, Spain with heterogeneous vegetation cover. The filter methods that were compared were: color-based filtering using an excessive greenness vegetation index (VI), Triangulated Irregular Networks (TIN) densification from LAStools, the standard method in Agisoft Photoscan (PS), iterative surface lowering (ISL), and a combination of iterative surface lowering and the VI method (ISL_VI). Results showed that for bare areas there was little to no difference between the filtering methods, which is to be expected because there is little to no vegetation present to filter. For areas with shrubs and trees, the ISL_VI and TIN method performed best. These results show that different filtering techniques have various degrees of success in different use cases. A default filter in commercial software such as Photoscan may not always be the best way to remove unwanted vegetation from a point cloud, but instead alternative methods such as a TIN densification algorithm should be used to obtain a vegetation-less Digital Terrain Model (DTM).

Keywords: UAV; fixed-wings; low-altitude aerial photography; DTM; vegetation filtering; TIN densification; sparse vegetation

1. Introduction

Digital Elevation Models (DEMs) are 3D representations of the Earth's surface. DEMs have numerous applications in for example: geomorphology, hydrology, ecology and other natural sciences. DEMs are used for, e.g., resource patch connectivity in ecology [1], geomorphometrical analyzes of the landscape [2,3] and modelling of water and sediment flows [4,5]. For many of these applications it is important to have high-resolution, high quality DEMs to be able to quantify and model relevant processes at both large and small scales.

LiDAR (Light Detection And Ranging) is one of the most widely used techniques to acquire point clouds for the creation of DEMs [6]. With LiDAR, a laser scanner is positioned on a satellite, aircraft/helicopter, boat/vehicle or tripods which measures the travel time between emission and reception of a laser pulse after it was reflected by an object. The strength of the returned signal provides information on the characteristics of the object, and is used to e.g., classify points representing, among others, bare ground, vegetation, water or human infrastructure. Classified point clouds help to analyze the object of interest, speed up calculations and reduce noise. For example, when vegetation points are separated from ground points, only these ground points can be used to interpolate into a continuous surface of the terrain without vegetation, i.e., a Digital Terrain Model (DTM). When extracted from the vegetated surface (DSM, Digital Surface Model), DTMs can be used to estimate vegetation height (Canopy Height Model, CHM) and derivatives such as total aboveground biomass [7]. Although LiDAR is extremely useful, the acquisition of airborne laser scans is expensive.

DTMs themselves are valuable tools to model geomorphological and hydrological processes. For the purpose of such analyzes, it is important to retrieve the actual terrain surface, and not the vegetated surface. In surface models, trees and shrubs are represented as impenetrable obstacles, while in reality water and sediment flows around the stems of such vegetation. Modelling hydrological behavior and/or sediment transport with surface models will likely to lead to wrong assumptions.

Aerial photogrammetry is an alternative technique to create DEMs. On the basis of overlapping images common points are identified that, with known camera specifications, can be positioned in 3D space. Unmanned Aerial Vehicles are nowadays popular tools for the acquisition of aerial photographs. These photos provide the data for post-processing algorithms such as Structure-from-Motion (SfM) photogrammetry and Multi-View Stereo (MVS) to derive very detailed point clouds of an object or surface [8,9]. SfM-MVS requires a higher percentage of overlap in the images to have many shared image points compared to traditional photogrammetry. On the other hand, due to the high data density, SfM-MVS is fully automated and is able to produce very dense point clouds. These photogrammetric point clouds are not only the basis of 3D surface reconstructions, but also for generating orthorectified mosaics. This allows generating very high-resolution elevation data and imagery efficiently.

A variety of methods exist to classify points as bare ground or vegetation of LiDAR point clouds [10]. Many such methods use several iterations of interpolation, classifying points above the interpolated surface as non-ground or vegetation, and interpolate again with a new selection of potential ground points. These interpolations can be based on a raster with regularly spaced grid cells such as the iterative surface lowering (ISL) algorithm of [11] and [12] or based on triangulated irregular networks (TIN) such as an implementation in the popular LAStools [13–15].

The abovementioned filtering techniques are widely used to process LiDAR data but may not be directly applicable to photogrammetric point clouds. A laser pulse is able to penetrate partly through the vegetation layer, generating actual ground points below a vegetated surface. Aerial photographs do not contain information below dense vegetation, hence there are very few or no ground points in such areas. The result is that points in a photogrammetric point clouds are often more clustered, which may affect the accuracy of ground point classification using existing methods. On the other hand, points obtained using SfM do contain color information that can potentially be used for filtering of vegetation.

Even though the use of SfM for obtaining DEMs and DTMs has increased substantially over the years, comparing different techniques for the separation of bare ground and vegetation from point clouds remains a difficult issue. Some studies looked at the enhancement of DTMs by classifying vegetation [16] using the grid cells. Other studies use filtering algorithms that are readily available in (commercial) software packages like Agisoft Photoscan [17], however, estimates on errors of these filtering techniques [18] were not mentioned. Also, new techniques or algorithms have been introduced by others, but they do not compare their algorithms to already existing algorithms [19], or only verify the reproducibility of the methods for different areas, while not actually considering vertical errors in DTMs [20]. [21] compared the classification results of different filtering algorithms, but only assessed

overall vertical errors of the best performing method. Without such a comparison, it is difficult to choose which technique is most appropriate for different settings, locations and DTM applications.

Therefore, the objective of this paper was to compare multiple vegetation filtering algorithms for the classification of point clouds in an area which is heterogeneous in terms of vegetation for creating DTMs. The study site was an area in SE Spain with a Mediterranean climate, because the area includes a combination of sparse and dense vegetation, with bare ground, shrubland areas and forested areas, which ensures proper testing of all involved algorithms.

2. Methods

2.1. Study Area

The study was carried out in the Guadalantin basin, approximately 70 kilometers west of Murcia City (Figure 1). The area has a Mediterranean climate, with mean annual precipitation of 320 mm (measured at the nearby Valdeinfierno reservoir [22]. The natural vegetation in the study area has been characterized as the Meso-Mediterranean Murcian-Almerien vegetation series [23]. The area is dominated by grasses and shrubs *Stipa tenacissima*, *Thymus vulgaris*, *Rosmarinus officinalis*, *Antyllis cystisoides* and *Helictotrichon filifolium* [23–26]. Trees are not as abundant as shrubs, and occur mainly on north-facing slopes. Tree types are *Quercus coccifera*, *Rhamnus lycioides* and *Pinus halepensis*.

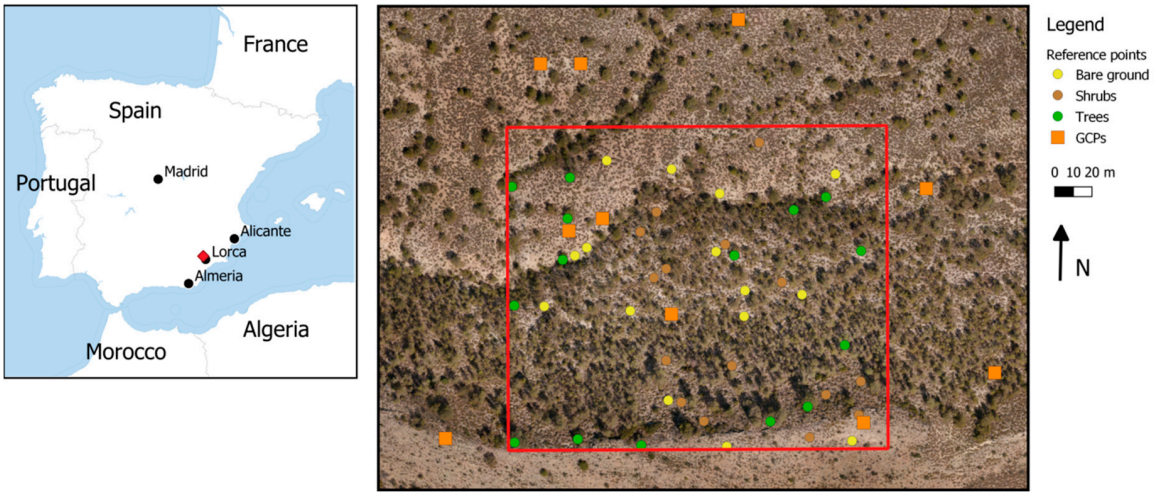

Figure 1. The study area in the Guadalantin Basin near Lorca and Murcia, Spain. The right inset shows the spatial distribution of ground control points and reference points.

2.2. Unmanned Aerial Vehicle, Camera and Photo Processing

A fixed-wing Mavinci Sirius 1 Unmanned Aerial Vehicle (UAV) with a wingspan of 1.6 m and a maximum take-off mass of 2.6 kg was used to obtain aerial photographs. A Panasonic Lumix GX1 16 MP camera (focal length 20 mm, aperture F1.7, exposure time 1/1600) was mounted on the aircraft to collect JPEG images at approximately 2 frames per second. Average ground speed of the UAV was 60 km/h, depending on wind direction and thrusts.

The average flight altitude for this study was set at 100 meters but varied because of relief. This resulted in photographs with a ground sample distance (GSD) of 2 cm on average. The flight lines were programmed for the images to have 85% overlap in flight direction and 60% side overlap. A point cloud was created from the resulting photographs using Agisoft Photoscan [17], with a workflow as described in [27]. Photoscan processing quality can be configured to low detail/fast processing to very high detail/intense processing. "High" detail is considered optimal for creating landscape reconstructions and DEMs—although the highest setting produces a more dense point cloud, it also introduces more noise. Generally, the highest processing setting is more suitable for 3D object reconstructions using

close-range photogrammetry. Moreover, "aggressive depth filtering" was configured for dense point cloud processing. Other than this, default Photoscan settings have been used.

In total 15 ground control points (GCPs) were positioned spatially well-distributed throughout the study area at relatively low, medium and high locations. The GCPs consisted of 80 × 80 cm orange textile rectangles, with inside a 30 × 30 cm black textile square with a CD disc on top. The coordinates of the center point of the CD disc were measured with a TopCon HIPer Pro GNSS RTK receiver. The orange squares and CD discs allowed the GCPs to be identified easily and the measuring point could be determined accurately. These points have been used to re-align the point cloud in Photoscan for more accurate georeferencing.

2.3. Filter Algorithms and Point Cloud Interpolation

Many algorithms for filtering of ground points for LiDAR point clouds exist already and more are being developed [28]. We selected five different filtering algorithms and tested their performance on filtering UAV point clouds. The selection was based on popularity, availability of existing tools and presence of literature:

1. Ground point classification based on a vegetation index (VI), particularly the excessive greenness as calculated from the RGB color values
2. TIN densification, or Adaptive TIN, as implemented in LAStools (TIN), [21,29]
3. Photoscan native filtering algorithm (PS) [18]
4. Iterative surface lowering (ISL) which resembles the algorithm described by [11]
5. A combination of ISL and VI (ISL_VI).

The different methods are described in detail below.

2.3.1. Filtering based on Excessive Greenness Index

Earlier research showed that image classification can help filter out vegetation points from point clouds [30]. Aside from (x, y, z) coordinates, many point clouds also contain color values that could potentially be used to classify points, for example, by using thresholds of absolute color values or via vegetation indices. Vegetation indices are combinations of spectral band values formed using mathematical equations designed to emphasize response to some vegetation property. Such indices are widely used for vegetation analysis such as drought and health estimations as well as land use/cover classification. More specifically, vegetation indices are used to differentiate image pixels with vegetation information from other pixels such as bare ground, infrastructure or clouds. Hence, vegetation indices are potentially useful for the identification of vegetation points and filtering them out of point clouds.

There are many vegetation indices for a wide variety of purposes, of which most effective are calculated based on green, red, red-edge, near-infrared and/or infra-red bands, such as the Normalized Difference Vegetation Index (NDVI) and the Enhanced Vegetation Index (EVI). Remote sensing equipment has dedicated sensors that are sensitive to these spectra.

On light-weight UAVs such as the one used in this study, the maximum payload is limited, hence the type of sensors on board are restricted by their weight. While multi-spectral cameras are becoming lighter and nowadays there are versions that can be integrated into a small aircraft (e.g., Parrot Sequoia), many UAVs are still equipped with a simple consumer photo camera. Such cameras are typically equipped with CMOS sensors that are sensitive to visible light until near-infrared (NIR) (400–900 nm) with RGB channels and filters to block radiation above 650 nm.

Such cameras can be modified to remove filters for dedicated spectral bands such as NIR, but by doing so these cameras lose their capabilities for accurate measurements of red light that is also required for many vegetation indices.

There are vegetation indices based on only bands in the visible light. Examples are the Visible Vegetation Index (VVI, Equation (1)) and Excessive Greenness (ExG, Equation (2)) which can be used

to separate vegetation from a background of bare ground. VVI is an index between 0–1 where values close to zero indicate bare ground and higher values indicate vegetation.

$$VVI = \left[\left(1 - \left|\frac{R - R_0}{R + R_0}\right|\right) \times \left(1 - \left|\frac{G - G_0}{G + G_0}\right|\right) \times \left(1 - \left|\frac{B - B_0}{B + B_0}\right|\right)\right]^{\frac{1}{W}} \quad (1)$$

R, G and B are the values of the red, green and blue channels, RGB_0 is the vector of the reference green color (in this study $R_0 = 40$, $G_0 = 60$, and $B_0 = 10$), and w is a weight component (here 1) [31]. ExG is a continuous index where higher values represent bright green reflecting surfaces such as vegetation, and low values indicate bare ground or obstacles.

$$ExG = 2G - R - B \quad (2)$$

Where R, G, B values are normalized values of the red, green and blue bands. In this study we calculated and visually compared the contrast and how much the vegetation could be recognized. We found that VVI was most useful for recognizing subtle differences between types of vegetation, and with ExG there was a higher contrast between vegetation and bare ground. Since the purpose was to classify vegetation points and ground points, ExG was the index of choice. During filtering we removed any point with $ExG > 0.1$ from the point cloud.

2.3.2. TIN Densification

TIN densification is a method based on Triangulated Irregular Networks. First, a sparse TIN is created based on a minimum number of points. Then points are iteratively added to the TIN to create a more detailed (densified) TIN, if the points meet certain criteria of the triangle (e.g., distance to TIN facets) within a given threshold. Thresholds were automatically derived and updated after each iteration. All rejected points are considered not part of the ground surface, such as vegetation or some other obstacle. For more information we refer to [10,14,15,32].

LAStools [13] comprises a collection of command-line tools for processing point cloud data, including an implementation of ground point filtering using TIN densification. In this test case we used LAStools, in particular the lasground_new.exe to filter out ground points. The exact implementation of the TIN densification is unknown since LAStools is proprietary software.

2.3.3. Agisoft Photoscan Native Filtering Algorithm

Agisoft Photoscan is a popular all-in-one package for processing aerial imagery into point clouds, DEMs and orthorectified image mosaics, which was also used in this study for generating the point cloud. Photoscan includes a native implementation of ground point filtering which allows tuning threshold parameters related to max angle between the terrain model and line to connect the point (15 degrees, higher values may improve results in steeper areas), max distance between the terrain model and a point (1 m) and cell size of the intermediate terrain model (5 m, this reflects the max expected data gaps due to buildings or tree cover). The parameter settings were manually optimized to produce, visually, best results. Result could improve by further understanding of the closed-source implementation of the algorithm and, at least to some extent, automated parameter optimization.

2.3.4. Iterative Surface Lowering (ISL)

We implemented the method of [11], an iterative surface lowering algorithm using python scripting. ISL is comparable to TIN densification in the way that it iteratively changes a preliminary surface based on a varying subset of included points. In the first iteration all points are interpolated into a regularly gridded raster with a given cell size (1 m). All points above the surface are labelled as vegetation points, all points below the surface are labelled as ground points. In subsequent iterations, only ground points are included to the surface interpolation. When no more points change labels, the interpolated surface is stable and assumed to represent ground surface. The one meter cell size

was chosen based on manual heuristics; smaller cell size introduced more noise, and larger cell sizes reduced detail because too many points were removed.

2.3.5. ISL + VI

The ISL method can easily be extended with other filtering methods. In this test case we first removed vegetation points using the VI method described in Section 2.3.1, and used the selection of ground points as starting point of the ISL method.

2.3.6. Output

Each of the five test runs produced a classified point cloud and a number of rasters with 25 × 25 cm grid cells. While this resolution is considerably coarser than the original GSD of 2 cm, the filtering of vegetation points substantially reduces the point density, producing significant data gaps below dense vegetation. We found that finer resolutions produced too many interpolation artefacts. This cell size was considered optimal for the point density after classification, providing relevant details in the derived rasters while computing time was acceptable. The produced raster were:

- DSM: average elevation of all points inside grid cell boundaries
- DTM: average elevation of all ground points inside grid cell boundaries
- VI: average ExG values of all points inside grid cell boundaries
- VIground: average ExG values of all ground points inside grid cell boundaries
- Image mosaic: average color values of all points within grid cell boundaries

Existing gaps in the rasters were filled using Inverse Distance Weighting (IDW, weight = 1/distance^2) interpolation. We chose IDW interpolation because of the balance between efficiency and accuracy. IDW seemed to provide better results than e.g., bilinear or splines. More complex interpolations such as natural neighbors and kriging were computationally too demanding for the large number of points. However, other or optimized interpolations may produce better results. Nevertheless, it is beyond the scope of this paper to fully analyze effects of different interpolation techniques.

Moreover, we created another DEM by using only the lowest available point within the boundaries of each 25 × 25 cm grid cell. As this is not truly a filtering method it is not listed as such. On the other hand it could be a simple method to remove vegetation points. This DEM is included in the comparison with the other DEMs and is mentioned as LOW in the tables and figures.

2.4. Error Assessment of Resulting DTMs

Reference points were manually created and randomly distributed throughout the area (Figure 1). In total 15 points per vegetation categories (bare ground, shrubs and trees) have been created, totaling 45 reference points. The DSM formed the basis on the elevation of the reference points. For bare ground points, the values were directly derived from the DSM. The ground surface elevation below shrubs and trees (where DSM values represent vegetation height) were manually estimated using multiple cross section profiles of the DSM and visual extrapolation of ground surface elevation using a profiling plugin in QGIS software.

2.4.1. Quantitative Error Assessment

The generated reference points for the abovementioned three vegetation categories were used to assess the vertical error in each of the DTMs. For visualizing the differences between the methods, boxplots were created. Furthermore, the difference of root mean square error between estimated terrain height and DTM value below the different vegetation types were compared.

For an assessment of accuracy and precision of the different methods, several statistical tests were performed on the absolute errors of the reference points. Accuracy is determined by how close the measured values are to the estimated values and the precision is a description of random errors in the measurements.

To test accuracy between the different methods, an ANOVA test was carried out on the absolute error values per reference point per land cover class. In case of significant differences between the groups, a post-hoc Tukey Honest Significance Difference (Tukey-HSD) test was done. This test shows pairwise if there are differences between the means of the absolute errors of the different filter methods.

The variance of the absolute error is a measure for the precision of the method, with a low variance indicating a high precision. To test for differences in the variance between the groups a pairwise test was done using Bartlett's test ($\alpha = 0.05$) and p values were adjusted using the Bonferroni method.

2.4.2. Qualitative Error Assessment

A qualitative error assessment of the filter methods was done by visually comparing 3D plots of filtered point clouds. This way, it was possible to assess the effects the filters have on the point clouds in a particular part of the study area and understand why false-positive vegetation points were undetected by the filtering algorithms.

Profiles were drawn on the DTMs to highlight the differences between them: on a linear hillslope with alternating bare and shrubs, a linear hillslope with alternating bare and shrubs with a single tree, a channel surrounded by vegetation, a patch of trees and a hillslope with multiple patches of trees. In addition to the reference DSM and the filtered DTMs, a LiDAR DTM was added to the profiles for comparison. The LiDAR DTM is interpolated from a point cloud from airborne laser scans (0.5 point/m^2; [33]) measured on bare areas and underneath shrubs and trees.

3. Results

3.1. Quantitative Comparison of Filter Methods

Table 1 shows the percentages of filtered points by the different filtering methods and the root mean square error (RMSE) compared to the reference points under different vegetation. The PS method removes the lowest number of points, while the ISL_VI method removes the highest number of points. The RMSE shows that for the bare areas there is little difference between the filter methods, while for the shrubs and trees these differences increase substantially.

Table 1. Number of points in point cloud per filter method and the percentage of the total amount of original points filtered for the three land cover classes for the different filter methods. Root mean square error (RMSE; m) is indicated for each of filter methods for each land cover class. The total number of points in the original point cloud was 31,974,733.

	Ground	Vegetation	% Filtered	Bare	Shrub	Tree
DSM	3.20×10^7	0	0.00	0.05	0.96	5.16
ISL	2.40×10^7	0.79×10^7	24.83	0.05	0.31	3.04
ISL_VI	1.40×10^7	1.79×10^7	56.18	0.05	0.29	2.94
LOW	3.20×10^7	0	0.00	0.08	0.44	4.47
PS	3.00×10^7	0.19×10^7	6.06	0.05	0.50	0.81
TIN	2.07×10^7	1.13×10^7	35.41	0.05	0.33	0.78
VI	1.70×10^7	1.50×10^7	46.80	0.05	0.89	4.89

The variation in the difference between the estimated elevation of the reference points and the interpolated DTMs show, similarly to Table 1, that there is little variation between the various filters for the bare areas, but more so in the shrubs and trees areas (Figure 2). The variations are largest for the trees land cover type. The TIN and PS methods seem to have the lowest error values as well as the smallest variances.

For the bare ground areas, there are no significant differences between the mean absolute errors (MAE; i.e., measure of accuracy) of the methods (Table 2). There are significant differences in the variance (i.e., measure of precision) between the LOW method and the other methods, with the LOW method having the highest variance (i.e., lowest precision). Similarly, for the shrubs areas, there are no

significant differences between the MAE of the different methods, while the DSM and VI methods have significantly lower precision. For the tree areas, there are significant differences in the MAE for the DSM, PS and TIN methods. The DSM MAE is significantly higher than the MAE of all other methods, except for LOW and VI. The TIN and PS methods have significantly higher accuracies than the DSM, VI and LOW methods. The TIN and PS methods have significantly higher precision than all other methods.

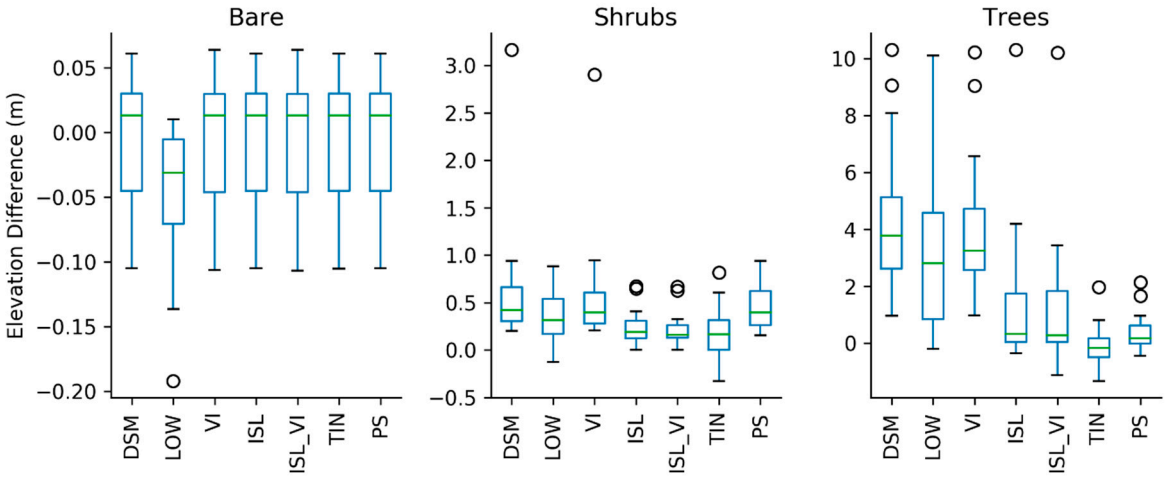

Figure 2. Boxplots for the three vegetation classes showing the elevation differences between the reference points and the interpolated digital terrain models (DTMs) after applying the filters.

Table 2. Pair-wise differences of the means of absolute errors of the reference DSM (in meters) and the various filtering methods, grouped by land cover class with p value of ANOVA testing. Positive numbers in the cells indicate the filter in the top row performs better; negative numbers indicate the filter method in the first column performs better. Post-hoc Tukey HSD test null hypotheses that were rejected ($\alpha = 0.05$) are highlighted. Variances between groups that differ significantly from Bartlett's test with Bonferroni adjustment are in bold.

	DSM	**ISL**	**ISL_VI**	**LOW**	**PS**	**TIN**	
DSM							
ISL	0						Bare $p = 0.99$
ISL_VI	0	0					
LOW	**0.009**	**0.01**	**0.009**				
PS	0	0	0	**−0.009**			
TIN	0	0	0	**−0.009**	0		
VI	0	0	0	**−0.009**	0	0	
DSM							
ISL	**−0.4074**						Shrubs $p = 0.017$
ISL_VI	**−0.4259**	**−0.0185**					
LOW	**−0.2873**	0.1201	0.1387				
PS	**−0.2008**	0.2066	0.2251	0.0865			
TIN	**−0.4038**	0.0036	0.0221	−0.1165	−0.203		
VI	−0.0417	**0.3657**	0.3842	**0.2456**	**0.1591**	**0.3621**	
DSM							
ISL	−2.8992						Trees $p < 0.001$
ISL_VI	−2.9337	−0.0346					
LOW	−1.025	1.8742	1.9087				
PS	**−3.8948**	**−0.9956**	**−0.961**	**−2.8698**			
TIN	**−3.8393**	**−0.9402**	**−0.9056**	**−2.8143**	0.0554		
VI	−0.2577	2.6415	2.676	0.7673	**3.6371**	**3.5816**	

3.2. Qualitative Comparison of Filter Methods

The removal of the filtered points is clearly visible in the colored point clouds (Figure 3). The filtered points can be seen as white gaps within the image. The images suggest that the ISL, VI_ISL and TIN methods filter the largest number of points, while the other methods filter relatively few (also see Table 1).

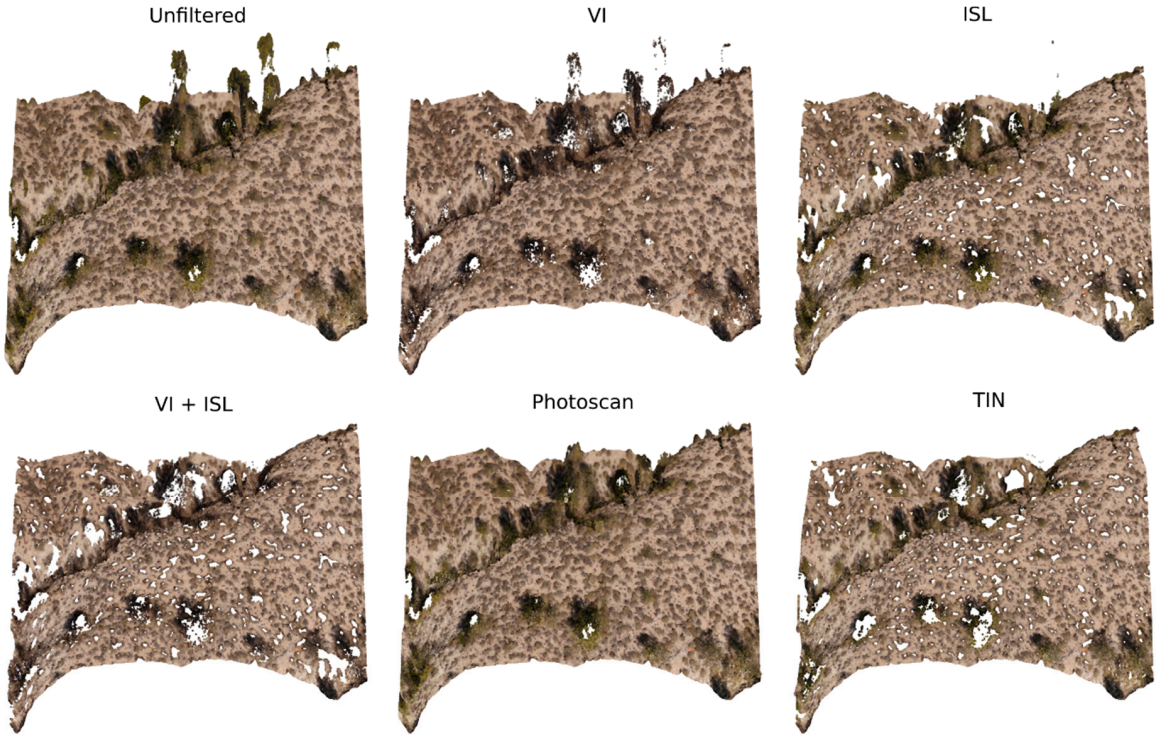

Figure 3. Colored point clouds showing the location of the filtered vegetation points for a subset area within the entire study area where a better filtering performance from the VI + ISL and TIN approaches can be observed.

When visually comparing the performance of the different filter methods, it becomes apparent that the VI_ISL and TIN methods remove most of shrub and tree points. The VI, ISL and PS methods leave many vegetation points after the filter procedure. Even the smaller tussocks are removed in the TIN and VI_ISL methods, while the other filter methods leave them largely unchanged.

The profiles (Figure 4) show a similar picture as the colored point clouds. For bare ground areas (B profile), there are only minor differences in elevation between the methods, while for shrubs (A profile) and trees (C–E profiles), these differences are much larger.

When looking at a single tree (Figure 4: D profile), all filter methods, except for the VI method remove the entire tree which is present in the original DSM. When looking at patches of trees (E profile) however, the only method that approaches the original LiDAR DTM is the TIN filter method. All other filter methods leave large parts of the trees intact, especially the large patch of trees at the top of the slope.

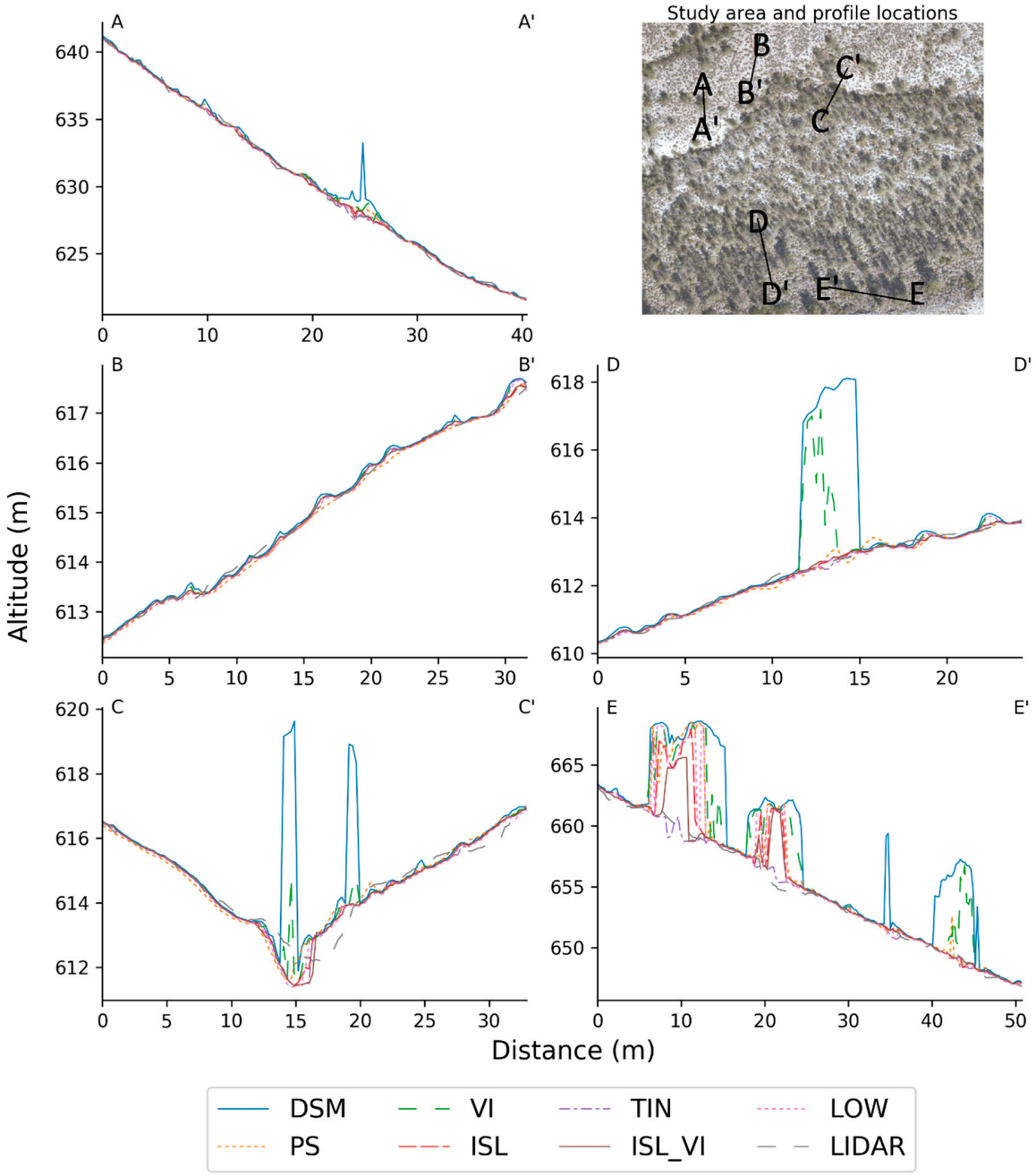

Figure 4. The profiles (Figure 4) show a similar image as the colored point clouds. For bare areas (**B** profile), there are only minor differences in elevation between the methods, while for shrubs (**A** profile) and trees (**C**–**E** profiles), these differences are much larger.

4. Discussion

4.1. Performance of Filter Methods

The filters that were used in this study all come with several pros and cons. For example: some filters are easily applied (TIN and PS), while for other algorithms there are no simple, straightforward tools available (ISL and VI). In this study we merely looked at the performance of the filters for different land cover types.

For the bare ground areas, there is hardly any difference between the different filter algorithms for the reference points (Table 2). Due to the limited amount of vegetation that could be removed in these areas, differences are also small. The same becomes apparent when looking at the colored point

clouds (Figure 3) and the profile of bare ground (Figure 4, profile B). This means that for bare areas, there is no need for the application of a filter. Controversially, applying a filter can provide worse results, as is the case here with the LOW filter. The LOW method uses the lowest point for each cell to calculate the height, which is prone to underestimation of the actual surface, especially when there is no vegetation present.

For the shrub areas, when looking at the reference points (Table 2), most algorithms perform similarly, except for the VI algorithm, which underperforms. Regarding the other algorithms, only the ISL_VI method has higher precision than the ISL method, which means that for shrub areas, the ISL_VI method is preferred over both the ISL as well as the VI method. However, when looking at the colored point clouds (Figure 3) and the profiles (Figure 4, profile A), both the ISL_VI and the TIN method perform best in removing shrubs from the point cloud.

For the tree areas, there are notable differences in the performance of the algorithms when looking at the reference points (Table 2). The PS and TIN method outperform all other methods, both in accuracy and precision. When looking at the colored point clouds and the profiles, however, the PS algorithm does not perform well. The ISL_VI algorithm filters trees better than the PS algorithm, and the TIN method filters out most trees and is similar to the surface of the LiDAR DTM (Figure 4, profile E).

The five different methods proposed in this study all reduce the error associated with the elevation of a terrain model beneath vegetation, but there are notable differences between the different algorithms. Overall the, TIN method performs best in all situations. Yet, we need to consider that PS filtering performance is underestimated due to poor filtering parameter settings. While considerable time was spent to manually optimize the parameter settings, there could be a better parameter set which might perform better in this study area.

4.2. Comparison of Filters to Previous Studies

The TIN filter method performed best in this study and showed RMSE values of 5 cm for bare ground areas, 33 cm for shrub areas and 78 cm for tree areas (Table 1). Most studies looking at filtering of vegetation do not report error values directly [20,34], which means the performance of the algorithms in our study area cannot be compared to their results. In studies where error values were reported, the errors are comparable to the ones found in this study. [21] reported RMSE values of 5 cm for flat terrain, 18.4 cm on sloping terrain and 22 cm in the vicinity of above-ground objects. However, this study was done in a more urban setting, and there is no reporting of RMSE values below vegetation. In a study by [29] DTMs were created for a vegetated area using LiDAR and SfM, and consecutively filtered using the same LAStools TIN method as in this study, showed that there was a mean difference of 9 cm between the two DTMs under the canopy. However, differences of > 50 cm also occurred. No comparison was made to actual measurements of ground level. The TIN method was also used by [34] who used this method with a single iteration to obtain a vegetation height model, to look at heights of shrub vegetation. Shrub vegetation heights measured on the ground were accurately represented using SfM point cloud data (r^2 = 0.96, SE = 8 cm, n = 31) and a combination of spectral and height predictor variables yielded an 11-class classification with 82% overall accuracy. There was no error assessment done on the (vertical) errors of the bare earth model. Due to the lack of error assessment, it is not clear what the real accuracy of the results of these studies really is.

4.3. Further Improvement of Filtering Methods

The VI and ISL_VI methods use color information from the points to classify vegetation points. We used photos from a standard RGB camera, while many UAV sensors have the capacity to record reflection in near-infrared (NIR). This NIR can be used to obtain more accurate classifications of vegetation, because of a very high reflectance of vegetation in these wavelengths.

Most of the algorithms that were used need some form of calibration through single or multiple parameter settings based on expert knowledge. In order to further improve such algorithms, measuring sufficient reference points during the flight campaigns could be used as input for calibration procedures

or automated parameterization. Such calibration procedures have the aim to minimize the error between the resulting DTM and the estimated reference points. A Monte Carlo-type approach can be used to obtain optimum parameter settings for the filter algorithms. [35] used a similar approach for modelling the vertical errors in DTMs obtained from LiDAR point clouds. This type of approach, however, needs to filter the raw point cloud and interpolate the entire DTM at each step. This makes the approach computationally expensive and time consuming.

4.4. Which Filter Should Be Used? Implications for Environmental Modelling

Many studies that use SfM to obtain DTMs make use of the off-the-shelf standard algorithm embedded in Agisoft Photoscan (e.g., [18]). These studies often focus at other aspects than the actual classification of vegetation or bare ground like assessing erosion and deposition. To properly assess erosion and deposition, a good DTM is vital, as is the assessment of the errors that might be present in the DTM due to vegetation. The quality of DTMs may influence the modelled connectivity of a landscape [36] and with that the pathways transported water and sediment will take. Yet, when modelling [37] these landscape processes, the DTM is something most researchers take as a given, and the accuracy is frequently not questioned. Therefore, possible mistakes are not taken into account or a standard smoothing algorithm is performed before the actual model runs are started. Therefore, the accuracy of a DTM and properly filtering the vegetation from the DSM is an essential procedure that needs to be carefully done.

Our results show that although the Photoscan filter method performs well on our reference points, the qualitative results show otherwise. We showed in this study that for bare ground areas, there is not any difference between the methods. In areas with many trees, the TIN algorithm performs best in removing vegetation. For areas with shrubs, the qualitative results showed that the TIN and ISL_VI algorithm perform best. Overall, the TIN filter algorithm performs best over the range of land cover types and is the preferred filter method. Moreover, this method is readily available in the LAStools software package and, therefore, needs little or no knowledge on algorithm development.

5. Conclusions

- To assess the best algorithm for filtering vegetation from a Digital Surface Model five methods for filtering vegetation from SfM point clouds were tested in an area in SE Spain with a Mediterranean climate. This area represents a combination of bare areas, shrubland areas and forested areas, which ensured proper testing of all involved algorithms.
- Results showed that for bare ground areas there was little to no difference between the filtering methods, which is to be expected because there is little to no vegetation present to filter. For shrub areas and tree areas, the ISL_VI and TIN method performed best.
- These results show that the off-the-shelf algorithms are not always the best way to remove unwanted vegetation from a point cloud, but instead custom algorithms such as TIN densification should be used to obtain a vegetation-less DTM.
- Choosing the right filtering technique for hydrological and sediment transport modelling is essential to obtaining correct modelling outputs. Mistakes in the input DTM may change the modelled connectivity of the landscape, which in turn influences calculations of water and sediment yields.

Author Contributions: Conceptualization, N.A. and R.M.; methodology, N.A. and R.M., and S.K.; software, N.A. and R.M.; validation, N.A. and R.M., and J.V.; formal analysis, all; investigation, N.A. and R.M., and S.K.; resources, S.K.; data curation, N.A. and R.M.; writing—original draft preparation, all; writing—review and editing, all.; visualization, J.V.; supervision, S.K. and J.V.; project administration, S.K.; funding acquisition, S.K.

Funding: This work was supported by the SPECTORS project (143081) which is funded by the European cooperation program INTERREG Deutschland-Nederland.

Acknowledgments: We would like to thank Erik Cammeraat for the organization and assistance of the field work, and two anonymous reviewers for improving this paper.

Conflicts of Interest: The authors declare no conflict of interest.

References

1. Squires, J.R.; DeCesare, N.J.; Olson, L.E.; Kolbe, J.A.; Hebblewhite, M.; Parks, S.A. Combining resource selection and movement behavior to predict corridors for Canada lynx at their southern range periphery. *Biol. Conserv.* **2013**, *157*, 187–195. [CrossRef]
2. Anders, N.S.; Seijmonsbergen, A.C.; Bouten, W. Geomorphological Change Detection Using Object-Based Feature Extraction From Multi-Temporal LiDAR Data. *IEEE Geosci. Remote Sens. Lett.* **2013**, *10*, 1587–1591. [CrossRef]
3. Sofia, G.; Hillier, J.K.; Conway, S.J. Frontiers in Geomorphometry and Earth Surface Dynamics: Possibilities, limitations and perspectives. *Earth Surf. Dyn.* **2016**, *4*, 721–725. [CrossRef]
4. Masselink, R.J.H.; Heckmann, T.; Temme, A.J.A.M.; Anders, N.S.; Gooren, H.P.A.; Keesstra, S.D. A network theory approach for a better understanding of overland flow connectivity. *Hydrol. Process.* **2017**, *31*, 207–220. [CrossRef]
5. Pandey, A.; Himanshu, S.K.; Mishra, S.K.; Singh, V.P. Physically based soil erosion and sediment yield models revisited. *Catena* **2016**, *147*, 595–620. [CrossRef]
6. Liu, X. Airborne LiDAR for DEM generation: Some critical issues. *Prog. Phys. Geogr.* **2008**, *32*, 31–49.
7. Eitel, J.U.; Magney, T.S.; Vierling, L.A.; Brown, T.T.; Huggins, D.R. LiDAR based biomass and crop nitrogen estimates for rapid, non-destructive assessment of wheat nitrogen status. *Field Crop. Res.* **2014**, *159*, 21–32. [CrossRef]
8. Turner, D.; Lucieer, A.; Watson, C. An automated technique for generation georectified mosaics from ultra-high resolution Unmanned Aerial Vehicle (UAV) imagery, based on structure from motion (SfM) point clouds. *Remote Sens.* **2012**, *4*, 1392–1410. [CrossRef]
9. Westoby, M.J.; Brasington, J.; Glasser, N.F.; Hambrey, M.J.; Reynolds, J.M. 'Structure-from-Motion' photogrammetry: A low-cost, effective tool for geoscience applications. *Geomorphology* **2012**, *179*, 300–314. [CrossRef]
10. Sithole, G.; Vosselman, G. Experimental comparison of filter algorithms for bare-Earth extraction from airborne laser scanning point clouds. *ISPRS J. Photogramm. Remote Sens.* **2004**, *59*, 85–101. [CrossRef]
11. Kraus, K.; Pfeifer, N. Determination of terrain models in wooded areas with airborne laser scanner data. *ISPRS J. Photogramm. Remote Sens.* **1998**, *53*, 193–203. [CrossRef]
12. Kraus, K.; Otepka, J. *DTM Modelling and Visualization-the SCOP Approach*; Photogrammetric Week 05; Fritsch, D., Ed.; Wichmann Verlag: Heidelberg/Berlin, Germany, 2005; pp. 241–252.
13. Isenburg, M. "Efficient LiDAR Processing Software" (Version 170511, Academic). Available online: http://rapidlasso.com/LAStools (accessed on 1 August 2014).
14. Axelsson, P. Processing of laser scanner data—Algorithms and applications. *ISPRS J. Photogramm. Remote Sens.* **1999**, *54*, 138–147. [CrossRef]
15. Axelsson, P. DEM generation from laser scanner data using adaptive TIN models. *Int. Arch. Photogramm. Remote Sens.* **2000**, *33*, 111–118.
16. Poli, D.; Soille, P. Digital Surface Model Extraction and Refinement through Image Segmentation – Application to the ISPRS Benchmark Stereo Dataset. *Photogrammetrie Fernerkundung Geoinf.* **2012**, 317–329. [CrossRef]
17. AgiSoft LLC. *Agisoft PhotoScan User Manual, Professional Edition, Version 1.4*; AgiSoft LLC: St. Petersburg, Russia, 2018.
18. Nadal-Romero, E.; Revuelto, J.; Errea, P.; López-Moreno, J. The application of terrestrial laser scanner and SfM photogrammetry in measuring erosion and deposition processes in two opposite slopes in a humid badlands area (central Spanish Pyrenees). *SOIL* **2015**, *1*, 561–573. [CrossRef]
19. Jensen, J.; Mathews, A. Assessment of Image-Based Point Cloud Products to Generate a Bare Earth Surface and Estimate Canopy Heights in a Woodland Ecosystem. *Remote Sens.* **2016**, *8*, 50. [CrossRef]
20. Becker, C.; Häni, N.; Rosinskaya, E.; d'Angelo, E.; Strecha, C. Classification of aerial photogrammetric 3D point clouds. In Proceedings of the ISPRS Hannover Workshop: HRIGI 17 – CMRT 17 – ISA 17 – EuroCOW 17, Hannover, Germany, 6–9 June 2017.
21. Serifoglu Yilmaz, C.; Gungor, O. Comparison of the performances of ground filtering algorithms and DTM generation from a UAV-based point cloud. *Geocarto Int.* **2016**, 1–16. [CrossRef]

22. Rodriguez-Lloveras, X.; Bussi, G.; Francés, F.; Rodriguez-Caballero, E.; Solé-Benet, A.; Calle, M.; Benito, G. Patterns of runoff and sediment production in response to land-use changes in an ungauged Mediterranean catchment. *J. Hydrol.* **2015**, *531*, 1054–1066. [CrossRef]
23. Alías-Pérez, J. *Project LUCDEME: Proyecto LUCDEME: Mapa de Suelos de Lorca-953 (Soil Map of Lorca-953, scale 1:100,000)*; ICONA, Universidad de Murcia, Ministerio de Agricultura Pesca y Alimentación: Madrid, Spain, 1988. (In Spanish)
24. López Bermúdez, F.; Albaladejo, J. Factores ambientales de la degradacion del suelo en el area mediterranea (Environmental factors of soil degradation in a Mediterranean area). In *Degradacion y Regeneracion del Suelo en Condiciones Ambientales Mediterraneas (Soil Degradation and Rehabilitation in Mediterranean Environmental Conditions)*; Albaladejo, J., Stocking, M.A., Díaz, E., Eds.; CSIC: Murcia, Spain, 1990; pp. 15–45. (In Spanish)
25. Pérez, A.; Martín, J.M.; Pérez, T.; Torres, M.; Fernández, A.; Burgos, R.; Madrona, M.T.; Valle, F.; Díaz, J.L. *Project LUCDEME: Proyecto LUCDEME: Mapa de Suelos de Velez Blanco-952 (Soil Map of Velez Blanco-952, scale 1:100,000)*; ICONA, Universidad de Murcia, Ministerio de Agricultura Pesca y Alimentación: Madrid, Spain, 1993. (In Spanish)
26. Rojo Serrano, L. Spanish national plan to combat desertification. In *Desertification in a European Context: Physical and Socio-Economic Aspects. Luxembourg, Report EUR 15414 EN*; Office for Official Publications of the European Communities: Luxembourg, 1995; pp. 357–358.
27. Anders, N.S.; Masselink, R.; Keesstra, S.D.; Suomalainen, J. High-res digital surface modeling using fixed-wing UAV-based photogrammetry. In Proceedings of the Geomorphometry 2013, Nanjing, China, 16–20 October 2013; pp. 16–20.
28. Meng, X.; Currit, N.; Zhao, K. Ground Filtering Algorithms for Airborne LiDAR Data: A Review of Critical Issues. *Remote Sens.* **2010**, *2*, 833–860. [CrossRef]
29. Wallace, L.; Lucieer, A.; Malenovský, Z.; Turner, D.; Vopěnka, P. Assessment of Forest Structure Using Two UAV Techniques: A Comparison of Airborne Laser Scanning and Structure from Motion (SfM) Point Clouds. *Forests* **2016**, *7*, 62. [CrossRef]
30. Yilmaz, V.; Konakoglu, B.; Serifoglu, C.; Gungor, O.; Gökalp, E. Image classification-based ground filtering of point clouds extracted from UAV-based aerial photos. *Geocarto Int.* **2016**, 1–11. [CrossRef]
31. Ponti, M.P. Segmentation of Low-Cost Remote Sensing Images Combining Vegetation Indices and Mean Shift. *Geosci. Remote Sens. Lett.* **2013**, *10*, 67–70. [CrossRef]
32. Zhao, X.; Guo, Q.; Su, Y.; Xue, B. Improved progressive TIN densification filtering algorithm for airborne LiDAR data in forested areas. *ISPRS J. Photogramm. Remote Sens.* **2016**, *117*, 79–91. [CrossRef]
33. PNOA. Plan Nacional de Ortofotografía Aérea. 2014. Data downloaded via Centro de Descargas of the Instituto Geografica Nacional. Available online: http://centrodedescargas.cnig.es/ (accessed on 2 August 2014).
34. Fraser, R.H.; Olthof, I.; Lantz, T.C.; Schmitt, C. UAV photogrammetry for mapping vegetation in the low-Arctic. *Arct. Sci.* **2016**, *2*, 79–102. [CrossRef]
35. Aguilar, F.J.; Mills, J.P.; Delgado, J.; Aguilar, M.A.; Negreiros, J.G.; Pérez, J.L. Modelling vertical error in LiDAR-derived digital elevation models. *ISPRS J. Photogramm. Remote Sens.* **2010**, *65*, 103–110. [CrossRef]
36. Keesstra, S.; Nunes, J.P.; Saco, P.; Parsons, T.; Poeppl, R.; Masselink, R.; Cerdá, A. The way forward: Can connectivity be useful to design better measuring and modelling schemes for water and sediment dynamics? *Sci. Total Environ.* **2018**, *644*, 1557–1572. [CrossRef] [PubMed]
37. Nunes, J.P.; Wainwright, J.; Bielders, C.L.; Darboux, F.; Fiener, P.; Finger, D.; Turnbull, L. Better models are more effectively connected models. *Earth Surf. Process. Landforms* **2018**, *43*, 1355–1360. [CrossRef]